



Research paper

Pharmacological characterization of the 3D MucilAir™ nasal model

Clément Mercier^{a,b,*}, Elodie Jacqueroux^{a,b}, Zhiguo He^{b,c}, Sophie Hodin^{a,b}, Samuel Constant^d, Nathalie Perek^{a,b}, Delphine Boudard^{a,b,e}, Xavier Delavenne^{a,b,f}^a INSERM, U1059, Dysfonction Vasculaire et Hémostase, Saint-Etienne, France^b Université de Lyon, Saint-Etienne F-42023, France^c Laboratoire de biologie, d'ingénierie et d'imagerie de la greffe de cornée, BiiGC, EA2521 Saint-Etienne, France^d Epithelix Sàrl, 14 chemin des aulx, CH-1228 Plan-les-Ouates, Geneva, Switzerland^e UF6725 Cytologie et Histologie Rénale, CHU de Saint-Etienne, Saint-Etienne, France^f Laboratoire de Pharmacologie Toxicologie Gaz du sang, CHU de Saint-Etienne, Saint-Etienne, France

ARTICLE INFO

Keywords:

MucilAir™

In vitro model

Nasal barrier

Drug delivery

ABC transporters

Bidirectional transport

ABSTRACT

The preclinical evaluation of nasally administered drug candidates requires screening studies based on *in vitro* models of the nasal mucosa. The aim of this study was to evaluate the morpho-functional characteristics of the 3D MucilAir™ nasal model with a pharmacological focus on [ATP]-binding cassette (ABC) efflux transporters. We initially performed a phenotypic characterization of the MucilAir™ model and assessed its barrier properties by immunofluorescence (IF), protein mass spectrometry and examination of histological sections. We then focused on the functional expression of the ABC transporters P-glycoprotein (P-gp), multidrug resistance associated protein (MRP)1, MRP2 and breast cancer resistance protein (BCRP) in bidirectional transport experiments. The MucilAir™ model comprises a tight, polarized, pseudo-stratified nasal epithelium composed of fully differentiated ciliated, goblet and basal cells. These ABC transporters were all expressed by the cell membranes. P-gp and BCRP were both functional and capable of actively effluxing substrates. The MucilAir™ model could consequently represent a potent tool for evaluating the interaction of nasally administered drugs with ABC transporters.

1. Introduction

Nasal delivery represents a highly effective route of administration for drugs requiring a quick onset of action. Nasal drug delivery offers several advantages over systemic administration, including reduced side-effects, avoidance of hepatic first-pass metabolism and rapid local absorption of drugs owing to the abundant vascularization and high permeability of the sizeable nasal mucosa [1].

The introduction of intranasal drug candidates requires the development of pre-clinical screening experiments to evaluate their permeability through the nasal mucosa [2]. Currently, Caco-2 intestinal cell line is the only FDA-approved predictive *in vitro* model to evaluate the absorption of drugs [3]. Considering the morphological and physiological differences with the nasal barrier, new models of nasal mucosa must be developed and characterized to evaluate the absorption of nasal drugs. In this context, several *in vitro* cellular models have been developed with the aim of closely mimicking the biology of the nasal

barrier. The use of immortalized nasal cell lines, such as the bovine turbinate (BT) [4], rat nasal squamous carcinoma (NAS 2BL) [5] and human nasal squamous carcinoma RPMI 2650 cell lines [6,7] represents a widespread approach. Despite some advantages, including high proliferation capacity and genetic homogeneity, immortalized cell lines are far from the human nasal epithelium in terms of biophysiology due to their weak differentiation ability [8]. To overcome these limitations, various *in vitro* models have evolved over the years, becoming increasingly complex and developing from submerged monocultures to three-dimensional epithelia cultured at the air-liquid interface. These latest models, available under the brand names EpiAirway™ (MatTek Corporation) and MucilAir™ (Epithelix), are constituted from primary human epithelial cells freshly isolated from nasal or bronchial biopsies [9]. These models accurately reproduce the biophysiology of human airway epithelia including the presence of a functional mucociliary system and the secretion of mucus in a homeostatic state [10].

Nasally administered drugs permeate through the nasal epithelium

* Corresponding author at: 10 rue de la Marandière, Faculté de Médecine, Saint-Priest-en-Jarez, France.

E-mail addresses: c.mercier@univ-st-etienne.fr (C. Mercier), elodie.jacqueroux@univ-st-etienne.fr (E. Jacqueroux), zhiguo.he@univ-st-etienne.fr (Z. He), sophie.hodin@univ-st-etienne.fr (S. Hodin), samuel.constant@epithelix.com (S. Constant), nathalie.perek@univ-st-etienne.fr (N. Perek), delphine.boudard@univ-st-etienne.fr (D. Boudard), xavier.delavenne@chu-st-etienne.fr (X. Delavenne).

<https://doi.org/10.1016/j.ejpb.2019.04.002>

Received 22 November 2018; Received in revised form 18 March 2019; Accepted 2 April 2019

Available online 03 April 2019

0939-6411/ © 2019 Elsevier B.V. All rights reserved.

principally via the transcellular route [11]. This route implicates transport of the drug substances across the lipophilic cell barrier which may involve specific interactions with ATP binding cassette (ABC) drug transporters [12]. These ATP-dependent active proteins participate in the efflux of xenobiotics from the cells [13], thereby greatly limiting the bioavailability of drugs intended for systemic circulation [14]. Functional expression of the main ABC transporters, namely P-glycoprotein (P-gp), Multidrug Resistance associated Proteins (MRPs) and Breast Cancer Resistance Protein (BCRP) has already been widely demonstrated in several physiological barriers, including the blood-brain-barrier [15] and the intestinal barrier [16]. The sparse data available concerning the human nasal epithelium reveal the expression of a wide range of ABC transporters [17,18]. Identification of these transporters in *in vitro* models of the nasal epithelium is therefore essential in order to anticipate their involvement in the bioavailability of locally administered drugs [19].

In addition to the functional expression of ABC transporters, *in vitro* models must, regardless of their origin, exhibit critical barrier properties that should be carefully investigated to determine their relevance for drug transport studies. These properties include the establishment of an adequate transepithelial electrical resistance (TEER) and the expression of tight and adherens junction proteins limiting the paracellular permeability of hydrophilic compounds [6]. We recently demonstrated that the RPMI 2650 model is not suitable for evaluating the efflux of therapeutic compounds mediated by ABC transporters [20]. Although the MucilAir™ model has been used to investigate the inflammatory response to aerosolized pollen [21] or the protective properties of xyloglucan [22], to the best of our knowledge few data are available concerning its barrier properties for drug absorption and both the expression and functionality of ABC efflux transporters are still unknown. This study therefore focuses on the original pharmacological characterization of the MucilAir™ nasal model in terms of barrier properties extended to the functional expression of ABC efflux transporters.

2. Material and methods

2.1. Culture of MucilAir™ tissues

The MucilAir™ nasal tissues were purchased from Epithelix (Geneva, Switzerland) and originated from a mixture of human nasal cells brushed from a pool of samples from 14 healthy donors grown on 6.5 mm Transwell® Polyester membrane with 0.4 µm pore size (Costar 3470, Corning, New-York, USA). In our study, the MucilAir™ tissues were transferred on receipt into 24-well plates filled with 700 µL of pre-warmed MucilAir™ (Epithelix) culture medium. The tissues were routinely cultured at 37 °C in a saturated (> 99%) humidity environment containing 5% CO₂. The medium was renewed every two to three days. The transepithelial electrical resistance (TEER) was measured as a standard indicator of tissue integrity. Measurements were made every two days using an EVOM® resistance meter and STX 2 electrodes (World Precision Instruments, Sarasota, USA). Blank filter values were subtracted, and the corrected values were calculated according to the surface area of the inserts (0.33 cm²).

2.2. Culture of Caco-2 cells

Caco-2 cells were purchased from the American Type Culture Collection (Rockville, MD, USA) and used as a pharmacological control model for protein mass spectrometry experiments. Caco-2 cells were grown in 25 cm² flasks until passage 23–30. The cells were maintained in culture medium consisting of Dulbecco's modified Eagle medium (DMEM) supplemented with 10% fetal bovine serum (FBS), 1% non-essential amino acids, 100 U/mL penicillin G, 250 ng/mL amphotericin B and 100 µg/mL streptomycin in a 37 °C, 95% relative humidity and 5% CO₂ atmosphere. Cells were seeded onto the membrane of the insert

filters (Falcon®, translucent polyethylene terephthalate (PET) membrane, 0.4 µm pore size, high-density, with a surface area of 0.3 cm²) in 24-well companion plates (Dominique Dutscher, Strasbourg, France) at a density of 1 × 10⁴ cells/well and cultured for 21 days. The culture medium was changed every 2–3 days.

2.3. Histological examination of MucilAir™ tissues

The study of MucilAir™ tissues focused on their morphological characteristics and cell composition. For this purpose, freshly excised inserts were bisected to allow histological staining of paraffin-embedded sections. Fully differentiated tissue cultures were rinsed in phosphate-buffered saline (PBS) and fixed by complete immersion in 4% formaldehyde for 20 min at room temperature. Fixed tissues were embedded in paraffin, sectioned and processed for staining with hematoxylin-eosin (HE) and alcian blue. Alcian blue staining was performed during 30 min at room temperature with 1% alcian blue in 3% acid acetic at pH 2.5. Several sections were cut from paraffin blocks using a microtome (Leica Jung RM2035). The sections were then deposited on glass slides, observed by light microscopy (Microscope Leica DMRB) and digitalized with a Nanozoomer (Hamamatsu Photonics).

2.4. MucilAir™ flow cytometric phenotypic analysis

MucilAir™ tissues were dissociated by incubating trypsin on both side of the inserts during 20 min at room temperature to obtain a cellular suspension, 100,000 cells being used for each staining procedure. The cell population was labelled with a specific anti-CLCA1.PE-Cyn5.5 polyclonal goat antibody (AC21-1575-16, Abcore) for goblet cells or with anti-β-tubulin.PE mouse monoclonal antibody (sc-5274.PE, Santa Cruz) for ciliated cells. Aliquots of 50,000 cells were analysed by flow cytometry. Sequential gating was performed. The FSC/SSC cytogram was used first to select viable cells, and second to distinguish specific cell populations. The gain setting was established by running unstained and isotype control cells (normal mouse IgG1.PE, sc-2866, Santa Cruz Biotechnology, and Lightning-link PE-Cyn5.5 tandem conjugation kit to goat IgG isotype control antibody, Innova Biosciences). Compensations were calculated by acquisition of fluorescent beads. Both percentage and geometric means of fluorescence were recorded. The results were expressed as the percentage of labelled positive cells. A FACS DiVa flow cytometer (BD Biosciences) equipped with an argon ion and He-Ne lasers was used. Data were analyzed using DiVa 5.03 software.

2.5. Immunofluorescence

In this study, we used an IF technique applicable to flat-mounted human tissue initially developed for the study of endothelial and epithelial tissues [23,24]. Briefly, MucilAir™ inserts were fixed in pure methanol or 1% paraformaldehyde (PFA) added on both sides for 30 min at room temperature (RT). PFA-fixed tissues were permeabilized with 1% Triton X-100 for 15 min at RT while methanol-fixed inserts were rehydrated three times for 5 min in PBS at room temperature. Non-specific binding sites were then blocked for 1 h at 37 °C in PBS containing 2% heat-inactivated goat serum and 2% bovine serum albumin. Following this blocking step, the inserts were cut into eight pie-shaped wedges and placed in 24-well plates. The primary antibodies (Table 1) were diluted 1/200 in the blocking buffer and incubated either for 1 h at 37 °C or overnight at 4 °C. Nonspecific rabbit and mouse IgG were used as primary antibodies for the negative controls. The secondary antibodies were diluted 1/500 in the blocking buffer and incubated with the insert fragments for 45 min at 37 °C. These antibodies comprised Alexa Fluor 488 goat anti-mouse IgG2b (A-21141, Thermo Fischer Scientific [TFS]), Alexa Fluor 488 goat anti-mouse (A-11029, TFS), Alexa Fluor 555 goat anti-mouse IgG1 (A-21127, TFS) or Alexa Fluor 555 goat anti-rabbit (A-21429, TFS). The nuclei were finally counterstained with 0.1 µg/mL 4',6-diamidino-2-phenylindole

Table 1
List of antibodies and reagents used for the immunostaining of MucilAir™ nasal tissues.

Category	Target	Source	Supplier	Reference	Fixatives	Dilution	Incubation time
Phenotyping	β-tubulin	mouse	Abcam	ab11315	Paraformaldehyde	1/200	60 min
	Actin	–	Abcam	ab176756	Paraformaldehyde	–	30 min
Junction proteins	ZO-1	rabbit	SantaCruz	sc-10804	Paraformaldehyde	1/200	60 min
	E-cadherin	rabbit	SantaCruz	sc-7870	Methanol	1/200	Overnight
	Occludin	rabbit	Abcam	ab31721	Methanol	1/200	Overnight
	Claudin-1	rabbit	Abcam	ab15098	Methanol	1/200	60 min
ABC drug transporters	P-gp	mouse	SantaCruz	sc-55510	Paraformaldehyde	1/200	60 min
	BCRP	mouse	SantaCruz	sc-58222	Methanol	1/200	Overnight
	MRP1	rabbit	Abcam	ab99531	Paraformaldehyde	1/200	60 min
	MRP2	rabbit	Abcam	ab172630	Paraformaldehyde	1/200	60 min

(DAPI) in PBS at RT for 30 min. The samples were rinsed three times in PBS between all steps, except between the blocking step and incubation with the primary antibodies. The insert fragments were finally placed on glass slides, submerged in Vectashield Mounting Medium (H-1000, Vector Laboratories) and covered with glass coverslips. Evaluations of each marker were repeated at least twice. All biomarkers were imaged using an inverted epifluorescence microscope IX81 (Olympus, Tokyo, Japan) equipped with CellSens imaging software (Olympus, Munster, Germany). To highlight the spatial localization of tight cell junctions and ABC transporters in MucilAir™ tissue, a FLUOVIEW FV1200 laser scanning confocal microscope (Olympus, Tokyo, Japan) equipped with FV10-ASW4.1 imaging software was used.

2.6. Paracellular permeability

The paracellular permeability of MucilAir™ model was assessed using the hydrophilic compounds sodium fluorescein (NaFlu) and 4.4 kDa fluorescein isothiocyanate-dextran (FITC-Dextran). The compounds were dissolved in Hank's balanced salt solution (HBSS) containing 1% HEPES (v/v) to a final concentration of 10 µg/mL and filled into the apical donor compartments, while HBSS containing 1% HEPES (v/v) alone was introduced into the basal receiver compartments. The inserts were then incubated for 2 h at 37 °C and the amount of the fluorescent marker compound reaching the basal compartment was evaluated using a fluorometer (Fluoroskan Ascent™, Thermo Fisher Scientific) with wavelengths set at 485/535 nm. The apparent permeability (P_{app}) was calculated according to the equation:

$$P_{app} = \frac{V}{C_i \times A} \times \frac{C_f}{\Delta t} \quad (1)$$

where V is the volume of the acceptor compartment (in cm³), C_i is the initial concentration of the test compound (in g/L or mol/L), A is the area of the insert (in cm²), C_f is the final concentration of the compound in the acceptor compartment (in g/L or mol/L), and t is the duration of the experiment (in seconds).

2.7. Bidirectional transport studies

We investigated the involvement of P-gp, BCRP and MRP1-2 in the active efflux of known substrates in MucilAir™ tissues using bidirectional transport experiments. Only inserts displaying a TEER above 200 Ω cm² were used. Rhodamine 123 (20 µM) was assessed as a P-gp substrate using verapamil (100 µM) as inhibitor. Chlorothiazide (100 µM) was assessed as a BCRP substrate using Ko143 (10 µM) as inhibitor. Methotrexate (100 µM) and probenecid (100 µM) were used as a broad-spectrum substrate and an inhibitor of MRPs, respectively.

All compounds were diluted either alone or with the associated inhibitor in HBSS transport buffer supplemented with 1% HEPES (v/v) and 1% DMSO (v/v). Prior to incubation, all solutions were pre-warmed to 37 °C and the pH was adjusted to 7.4. Each condition was evaluated in triplicate. Bidirectional transport assays were performed from the

apical to the basal compartment ($P_{app A \rightarrow B}$) and from the basal to the apical compartment ($P_{app B \rightarrow A}$) for 2 h at 37 °C. Following incubation, the amounts of chlorothiazide and methotrexate that had permeated through the model in both compartments were quantified by liquid chromatography-mass spectrometry (LC-MS). Permeation of rhodamine 123 was quantified using a fluorometer at 485/535 nm. The bidirectional permeability was calculated according to Eq. (1). Finally, to determine whether the test compound was actively effluxed by ABC transporters, its efflux ratio (ER) was computed using the equation:

$$ER = \frac{P_{app B \rightarrow A}}{P_{app A \rightarrow B}} \quad (2)$$

2.8. LC-MS analysis

Chlorothiazide and methotrexate were quantified using an Aquity UPLC system coupled with a Xevo TQ-D triple quadrupole mass spectrometer (Waters, Saint-Quentin-en-Yvelines, France). Compounds were detected by Multiple Reaction Monitoring (MRM). Negative ionization conditions were used for chlorothiazide (m/z 293.98 → 214.16) and positive ionization conditions for methotrexate (m/z 455.19 → 175.11). The internal standards (IS) were [²H₆]-salicylic acid (141.14 → 97.10) and [²H₃]-methotrexate (458.25 → 311.2) for chlorothiazide and methotrexate, respectively. The mobile phase was a mixture of (A) 0.1% formic acid in water and (B) 0.1% formic acid in acetonitrile. A gradient was applied to a BEH C18 column (50 mm × 2.1 mm × 1.7 µm) (Waters). The peak area ratios of the drugs and their respective IS were used to calculate drug concentrations.

2.9. Protein mass spectrometry

Protein mass spectrometry experiments were performed to investigate the relative abundance of phenotypic markers of nasal mucosa, tight junction proteins and ABC drug transporters in the nasal MucilAir™ model. The FDA-approved Caco-2 cell line was used as a pharmacological control as the only existing predictive *in vitro* model of intestinal drug absorption [3]. Briefly, cells were recovered from the insert filters by trypsinization and collected by centrifugation at 300g for 5 min. The membrane protein fraction was extracted using the MemPER Plus membrane protein extraction kit (Thermo Fisher Scientific, Waltham, Massachusetts, USA) according to the manufacturer's protocol. Briefly, cell pellets were washed in the cell wash solution and re-suspended in the permeabilization buffer. After a 10 min incubation at 4 °C with constant mixing, the cell lysates were centrifuged for 15 min at 16,000g. The supernatant containing cytosolic proteins was removed and the pellets were re-suspended in the solubilization buffer. The homogenate was incubated for 30 min at 4 °C with constant mixing and then centrifuged for 15 min at 16,000g. The supernatant containing the membrane protein fraction was collected. Protein concentration was measured using the Micro BCA protein assay kit (Thermo Fisher

Scientific). The Pierce Mass Spec sample prep kit (Thermo Fisher Scientific) was used for in-solution tryptic digestion. Briefly, 100 µg of the membrane protein fraction were prepared in 100 µL of cell lysis buffer. The mixture was reduced with 10 mM dithiothreitol (DTT) for 45 min at 50 °C and alkylated with 50 mM iodoacetamide (IAA) for 20 min at RT. The proteins were precipitated with acetone and then re-suspended in 100 µL of digestion buffer. The samples were digested with Lys-C (1:100) at 37 °C for 2 h then with trypsin (1:50) for 16 h at 37 °C. Each sample was desalted using the Pierce Peptide desalting spin column according to the manufacturer's protocol.

The samples were analyzed using an Ultimate U3000 liquid chromatography (Thermo) system (at a flow rate of 300 nL/min) on an Easy-spray C18 column 2 µm, 0.075 mm ID × 500 mm (Thermo Fisher Scientific) with a 150 min gradient. Mobile phase A was water with 0.1% formic acid, and mobile phase B was 80% acetonitrile with 0.08% formic acid. Peptides were eluted by a gradient from 2.5% to 40% B over 123 min, followed by a short wash in 90% mobile phase B before return to the starting conditions.

Mass spectrometry (MS) was performed using a Q-Exactive Plus spectrometer (ThermoFisher, San Jose, California, USA). After measurement of a precursor scan of intact peptides in the Orbitrap by scanning from m/z 375–1500 (with a resolution of 70,000), the 10 most intensely multi-charged precursors were selected for HCD analysis in the C-trap (with a resolution of 17,500 and a normalized collision energy of 27). Automatic gain control (AGC) targets were 3×10^6 ions for MS scans and 1×10^5 ions for MS/MS scans. The maximum injection time was 100 ms and dynamic exclusion for 30 s was used to reduce repeated analyses of the same components.

Data concerning the identification and quantification of peptides and proteins were analyzed using Proteome Discoverer® software version 2.0 (Thermo Fisher Scientific). R software was used for statistical analysis and graphic outputs.

3. Results

3.1. Morphological and phenotypic characterization of the MucilAir™ nasal model

We initially studied the morphology and cell composition of nasal MucilAir™ tissues (Fig. 1). Examination of alcian blue- and hematoxylin eosin (HE)-stained histological sections confirmed the pseudostratified organization of the tissues and the predominant presence of columnar ciliated cells bearing a differentiated apical cilium, organized in a clump extending into the lumen (Fig. 1A). The use of alcian blue allowed the staining of mucins and the subsequent visualization of elongated goblet cells enmeshed between ciliated cells with a large apical cup. Nuclei were tight and excluded at the basal pole. Goblet cells were distended by abundant blue secretory mucus granules into a typical cup-like shape. Basal progenitor cells were small, flattened, with a predominant nucleus and were in direct contact with the membrane of the insert. The thin and homogeneous fluorescent staining of β -IV tubulin, a major constituent of microtubules, confirmed the presence of apical cilia organized in clusters covering the major part of the epithelium (Fig. 1C). The ciliated and goblet cell populations were quantified by flow cytometry using the specific markers β -IV tubulin and CLCA1, respectively (Fig. 1B). Quantitative analysis showed $12 \pm 3\%$ CLCA1-positive cells versus $66 \pm 17\%$ β -IV tubulin-positive cells, corroborating the predominant presence of ciliated cells in the MucilAir™ model. Protein mass spectrometry analysis confirmed the expression of β -IV tubulin in MucilAir™ at the same level as in control Caco-2 cells (Fig. 5A). Interestingly, the abundance of the radial spoke head-like protein α 4 (RSPH4) was approximately 10-fold higher in MucilAir™ than in Caco-2 cells, further testifying to the presence of ciliated cells in the nasal model. Gut specific mucin-13 was 10-fold more abundant in Caco-2 cells than in MucilAir™. Conversely, the airway-specific proteins mucin-5AC and mucin-5B displayed a 100-fold

and 10-fold greater abundance, respectively, in the nasal model than in Caco-2 cells. Finally, the basal cell marker aquaporin-3 was strongly detected in MucilAir™, but only weakly detectable in Caco-2 cells whereas integrin α -6 abundance was nearly identical in the two models. Overall, the MucilAir™ nasal model exhibited the main characteristics of the human nasal epithelium in terms of histology and cell type composition.

3.2. Barrier properties of the MucilAir™ nasal model

In the second part of our study, we examined the barrier properties of the MucilAir™ nasal model. In this context, we investigated the expression of the tight junction proteins zonula occludens 1 (ZO-1), occludin and claudin-1, and the adherens protein E-cadherin, by IF (Fig. 2A). Overall, the four proteins were found to be homogeneously expressed over the entire epithelium in a connecting network. A bright and homogeneous signal of ZO-1 was localized at the cell membrane. Confocal observations revealed a clear apical expression of the protein in the superficial cell layer. As an associated component of tight junction complexes, claudin-1 showed a distribution pattern similar to that of ZO-1, characterized by apicolateral membrane localization only in the superficial cell layer. A different expression pattern was observed for occludin, which was not only expressed on the apical side but was also localized on the lateral membranes of all cell layers. Finally, E-cadherin staining revealed a subcellular localization similar to that of occludin. The four proteins were detected in mass spectrometry with different abundances depending on the model used (Fig. 5B). Claudin-1 showed a closely similar abundance in both models, whereas e-cadherin was detected to a slightly greater extent in Caco-2 cells. The greatest differences in abundance were observed for occludin and ZO-1, which both exhibited a 10-fold greater abundance in Caco-2 compared to MucilAir™. Claudin-3 and ZO-2 were detected at an identical level in both models while ZO-3 showed a slightly greater abundance in MucilAir™ than in Caco-2 cells. The average TEER of nasal MucilAir™ tissues ($316 \pm 31 \Omega \text{ cm}^2$) reflected the expression of tight junction complexes. Finally, the tightness of the MucilAir™ model was quantitatively evaluated using the hydrophilic compounds sodium fluoride (NaFlu) and 4.4 kDa Dextran (Fig. 2B). NaFlu showed an average permeability of $5 \times 10^{-6} \text{ cm/s}$ whereas the permeability of 4.4 kDa Dextran was almost 10-fold lower ($6 \times 10^{-7} \text{ cm/s}$).

3.3. Expression of ABC efflux transporters

We investigated the expression and subcellular localization of four ABC transporters, namely P-gp, MRP1, MRP2 and BCRP, in IF experiments using both epifluorescence and confocal microscopy (Fig. 3).

P-gp displayed a clear staining at the membrane of superficial cells with an expression characterized by bright multiple fluorescent spots covering the whole apical membrane of most cells, although some cells remained unlabeled. BCRP exhibited a less intense signal than P-gp with a homogeneous expression characterized by thin and continuous apicolateral membrane staining in the superficial cell layer of the MucilAir™ tissues. The MRP1 transporter showed an expression pattern nearly identical to that of P-gp with a distinct signal observed exclusively at the luminal side of the cells. Conversely, MRP2 exhibited a heterogeneous expression in cells, characterized by a subcellular localization throughout the cell membrane. All four transporters were detected in proteomic analyses with distinct abundance levels (Fig. 5C). Both P-gp and BCRP exhibited a 100-fold lower abundance in MucilAir™ than in the Caco-2 model. MRP2 was approximately 10 times as abundant in Caco-2 cells as in MucilAir™. Conversely, MRP1 displayed a greater abundance in MucilAir™ than in Caco-2. MRP3, MRP4 and MRP7 were detected at nearly the same level in both models.

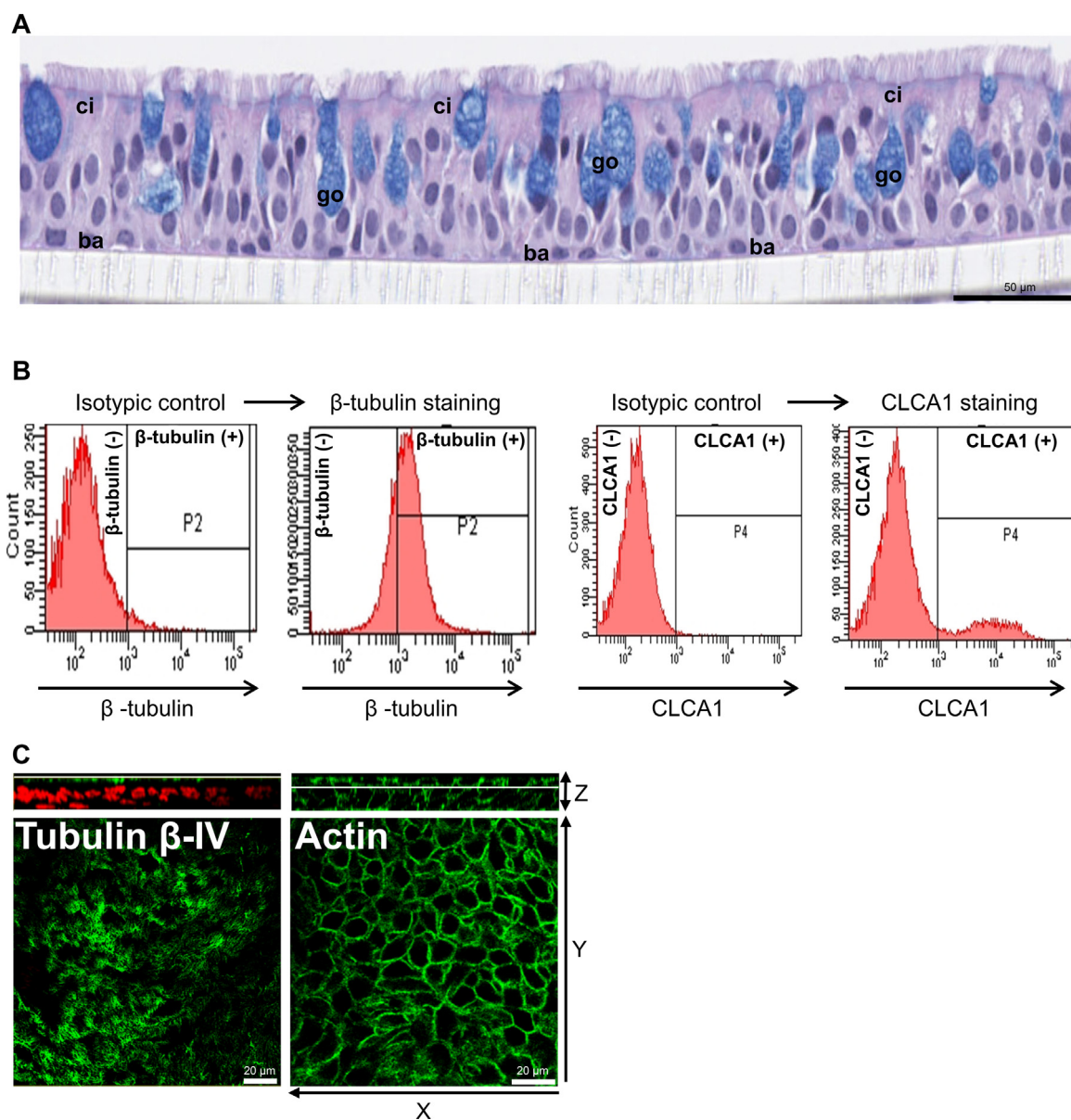


Fig. 1. Morphological and phenotypic characterization of the MucilAir™ nasal model. **A.** Hematoxylin-eosin (HE) and alcian blue-stained histological section. **ci:** ciliated cells, **go:** goblet cells, **ba:** basal cells. **B.** Quantitative flow cytometry analysis of the cell population. Isotypic phycoerythrin (PE) and PE.Cyn5.5 control acquisitions versus PE and PE.Cyn5.5 signals were performed for β -tubulin and chloride channel accessory 1 (CLCA1) markers, respectively. CLCA1 and β -tubulin immunostaining acquisitions were gated on the entire viable cell population; $n = 3$ for each condition. **C.** Immunofluorescence staining of β -IV tubulin and actin. Observations were performed using confocal microscopy. Nuclei were counterstained using 4',6-diamidino-2-phenylindole (DAPI).

3.4. Functionality of ABC efflux transporters

We subsequently evaluated the functional activities of P-gp, BCRP and both MRPs by performing standard bidirectional transport experiments (Fig. 4).

The functional activity of P-gp was examined using rhodamine 123 as a substrate, associated with the P-gp inhibitor verapamil (Fig. 4A). Rhodamine 123 exhibited a $P_{app(A > B)}$ of roughly 2×10^{-7} cm/s. The permeability of the compound in the basal to apical direction was found to be higher, around 1.2×10^{-6} cm/s, resulting in an efflux ratio of almost 6. The dissymmetric transport of rhodamine 123 was abolished in the presence of verapamil. Under these conditions, the $P_{app(B > A)}$ dropped to 2×10^{-7} cm/s whereas $P_{app(A > B)}$ remained unchanged and the ER was reduced by roughly 65% to nearly 2. P-gp was therefore functional in the MucilAir™ nasal model.

The functionality of BCRP was investigated using chlorothiazide and

Ko143 as the substrate and inhibitor, respectively (Fig. 4B). Chlorothiazide showed a differential transport through MucilAir™, characterized by a $P_{app(B > A)}$ 169% higher than the $P_{app(A > B)}$, leading to an ER of 2.7. The apical-to-basal permeability of chlorothiazide was not affected by the addition of Ko143 whereas the $P_{app(B > A)}$ was almost three times lower in the presence of this inhibitor, resulting in a halved ER. These results confirmed the involvement of BCRP in the active efflux of chlorothiazide and demonstrated the functional activity of this transporter in the MucilAir™ nasal model.

Finally, the functional activity of the MRP transporters was evaluated using methotrexate as a broad-spectrum substrate coupled with the wide-range MRP inhibitor probenecid (Fig. 4C). In contrast to rhodamine 123 and chlorothiazide, no dissymmetric transport was observed for methotrexate, which exhibited a nearly equally low permeability in both directions. The addition of probenecid did not change the bidirectional permeability of methotrexate and the consequent ER

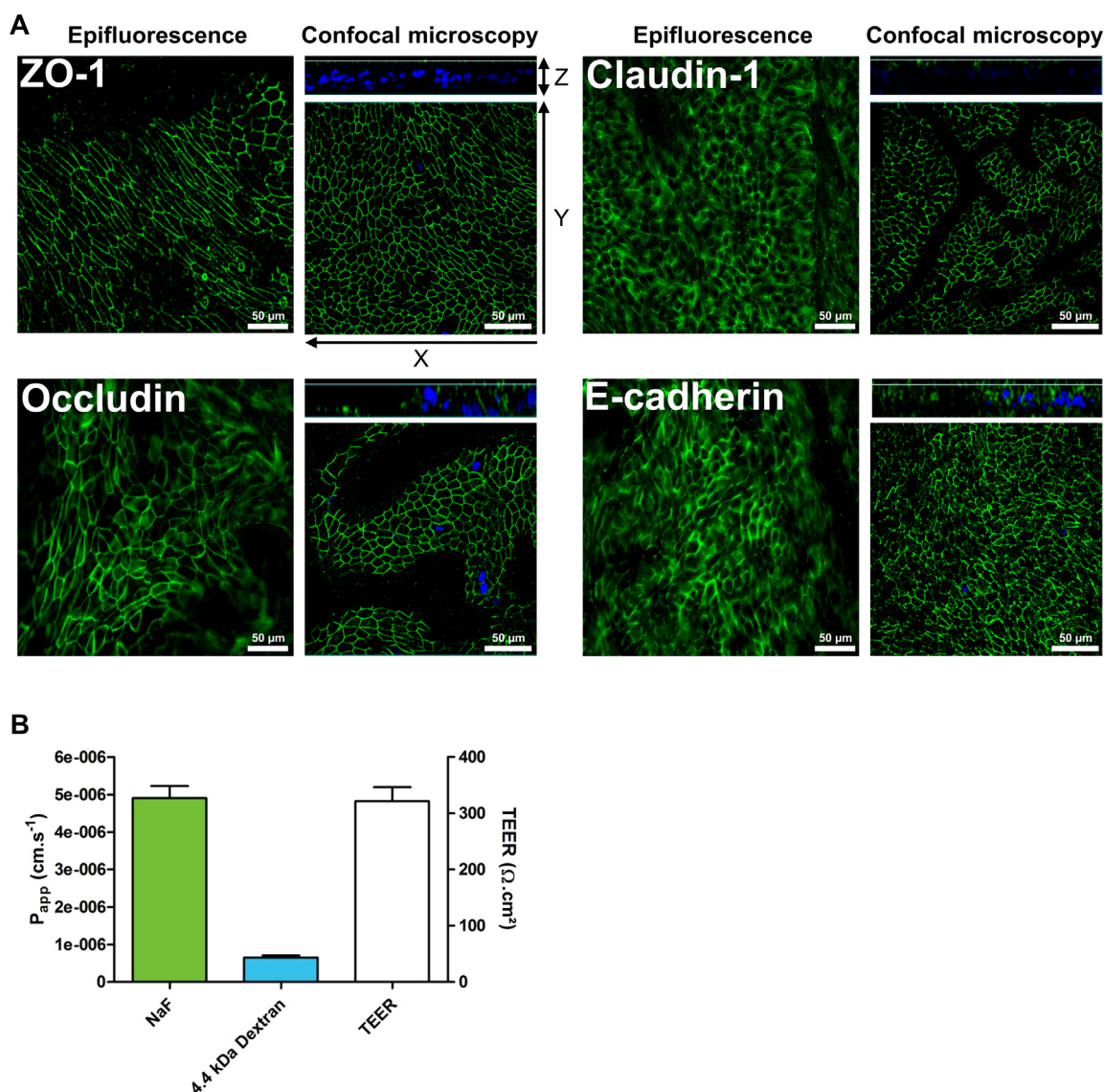


Fig. 2. Barrier properties of the MucilAir™ nasal model. **A.** Immunofluorescence staining of the tight junction proteins zonula occludens 1 (ZO-1), occluding and claudin-1, and the adherens protein e-cadherin, in the MucilAir™ nasal model. Observations were performed using epifluorescence (left) and confocal microscopy (right). Nuclei were counterstained using 4',6-diamidino-2-phenylindole (DAPI). **B.** Transepithelial electrical resistance (TEER) of the MucilAir™ nasal model ($n = 6$) and permeability of NaFlu/4.4 kDa dextran following 2 h of incubation ($n = 3$). Data are expressed as the mean \pm standard deviation.

remained below 2. The MRPs tested were therefore not involved in the active efflux of methotrexate in the MucilAir™ model.

4. Discussion

The efficacy of many drugs depends on their ability to cross tissues to reach their target. The efflux process mediated by ABC transporters plays a critical role in limiting the absorption and accumulation of exogenous compounds, which can lead to drug resistance. These membrane proteins are therefore key determinants of the pharmacokinetic and bioavailability profiles of locally administered drugs. At an early stage of drug development, *in vitro* models represent valuable tools for quickly assessing drug interactions with membrane transporters in pre-clinical studies [8,25]. Our study focused on the morpho-functional characterization of the MucilAir™ nasal model based on its barrier properties with a pharmacological extension to the expression and functional activity of well-known ABC transporters.

We initially examined the morphological appearance and cell phenotype organization of MucilAir™ nasal tissues. The human nasal mucosa comprises a pseudostratified respiratory epithelium supported by a

lamina propria. The nasal epithelium is composed of three types of cell including differentiated ciliated epithelial cells, goblet cells that produce mucus and basal cells involved in epithelium renewal. IF studies of β -IV tubulin, a major constituent of motile cilia [26], showed the presence of several cilia clusters sheathed in the apical membrane as previously described in the normal nasal mucosa [27]. Protein mass spectrometry was performed to investigate the abundance of specific phenotypic markers of nasal mucosa in the MucilAir™. Caco-2 intestinal model was used as a positive control for the validation of the proteomic method. Despite a preferential expression in cilia, the abundance of β -IV tubulin was similar in both MucilAir™ and Caco-2 models. This could be explained by the involvement of β -IV tubulin as one of the major constituents of ubiquitous cytoskeleton microtubules [28]. However, the greater abundance of RSPH4 in MucilAir™ than in Caco-2 cells was specifically related to the presence of ciliated cells. This protein is exclusively located in the head complex of cilia radial spokes involved in the transmission of regulatory signals in the ciliary beating process [29]. The presence of goblet cells was demonstrated by staining with alcian blue, a dye routinely used to stain mucins [30]. As expected, the abundance of mucin-5B and mucin-5AC was greater in MucilAir™ than

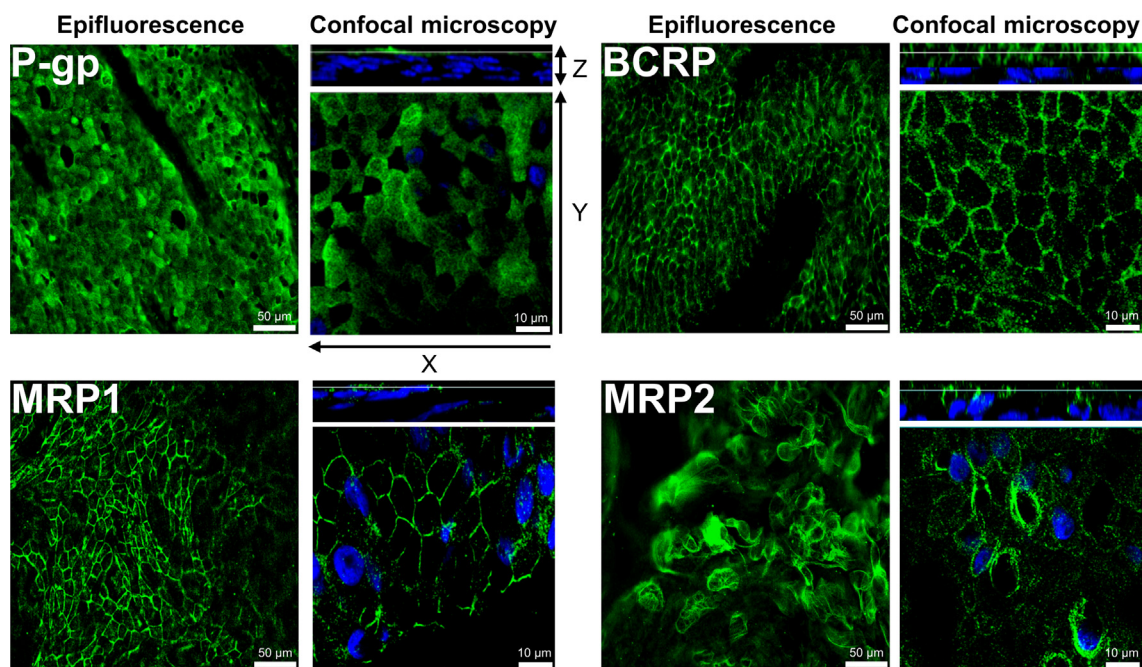


Fig. 3. Immunofluorescence staining of [ATP]-binding cassette (ABC) efflux transporters P-glycoprotein (P-gp), multidrug resistance-associated protein (MRP1, MRP2) and breast cancer resistance protein (BCRP) in the MucilAir™ nasal model. Observations were performed using epifluorescence (left) and confocal microscopy (right). Nuclei were counterstained in blue using 4',6-diamidino-2-phenylindole (DAPI).

in Caco-2 cells, these proteins being the main gel-forming mucins secreted in the upper airway [31]. Also, as expected, mucin-13 was more abundant in Caco-2 cells than in MucilAir™, in line with its preferential expression in intestinal mucus [32]. The proportion of each cell type was in accordance with *in vivo* observations indicating up to 50–80% of ciliated cells [33] and 15% of goblet cells in the nasal epithelium [34]. Basal cells are expected to cover approximately 5–10% of the nasal epithelium [35]. The presence of basal cells in the MucilAir™ model was supported by the expression of aquaporin-3, Kreda et al. having shown that aquaporin-3 is exclusively expressed in basal nasal cells [36]. Overall, the MucilAir™ nasal model was close to the normal human nasal epithelium in terms of cell type composition and histology.

One of the main functions of nasal epithelium is to act as a physical barrier against pathogens, allergens and air pollutants [37]. The integrity of the nasal epithelium is principally ensured by the presence of both tight and adherens junctions [38]. Tight junction proteins form intercellular bridges between adjacent cells that modulate the paracellular passage of hydrophilic compounds [39], whereas adherens junctions are involved in the stabilization of cell–cell adhesion and polarity [40]. The MucilAir™ nasal tissues showed a typical apical expression of ZO-1, occludin, and claudin-1; three major constituents of tight junctions [41–43] as well as the adherens junction protein e-cadherin [44]. The apical expression of occludin and claudin-1 has been demonstrated in excised nasal mucosa [45]. Moreover, Ong et al. recently observed the apical expression of ZO-1 and e-cadherin in primary nasal cells [46]. Caco-2 cell line provided a positive control of the abundance of tight junction proteins in proteomics experiment. Indeed, the Caco-2 model was shown to be a tight and polarized barrier with a strong expression of junctional proteins, a critical requirement for drug transport studies [47]. The greater abundance of occludin and ZO-1 in the Caco-2 cell line compared to MucilAir™ could be related to the cell composition of the two models. An ultrastructural study showed that tight junctions around nasal goblet cells were discontinuous and fragmented [48]. Similarly, tight junctions have been shown to be leakier between enterocytes and goblet cells than between enterocytes [49]. Considering that the Caco-2 cell line is homogeneously composed of enterocytes, the lesser abundance of occludin and ZO-1 in MucilAir™

could be related to the presence of both goblet and ciliated cells. Proteomic analyses also revealed the presence of claudin-3 isoform, a constituent of tight junctions involved in the regulation of ion permeability [50], as well as ZO-2 and ZO-3, two tight junction-associated proteins [40]. Finally, the paracellular permeability of NaFlu through MucilAir™ was within the same range as that of excised human nasal mucosa [51]. As expected, 4.4 kDa dextran exhibited a lower permeability than that of NaFlu due to its higher molecular weight. Taken together, these results provide further evidence of the involvement and efficacy of tight junction complexes in selective regulation of the paracellular transport of hydrophilic compounds in the MucilAir™ nasal model. Moreover, a recent study described the ability of this model to discriminate the permeability of compounds according to their physicochemical properties. Hydrophilic compounds typically exhibited lower permeability than hydrophobic ones due to a preferential permeation through the more restrictive paracellular pathway [52].

The last step of the assessment of the barrier properties of MucilAir™ tissues led us to investigate the functional expression of ABC transporters P-gp, BCRP, MRP1 and MRP2. The Caco-2 model was used as a positive control of ABC transporters abundance in proteomics experiments. Indeed, Caco-2 model was previously validated for the *in vitro* evaluation of drugs as substrates or inhibitors of ABC transporters in pre-clinical screening studies [4,53]. The functional activity of the selected transporters was subsequently assessed using the FDA-approved bidirectional transport protocol [4,54].

P-gp is a glycoprotein widely expressed on the apical membrane of various tissues including the respiratory epithelium [55]. The MucilAir™ nasal model showed a homogenous and apical expression of P-gp. The same expression pattern has been previously described in normal nasal epithelium [17]. The relative abundance of P-gp was roughly 100 times lower in MucilAir™ than in the control Caco-2 model. This result was consistent with those of a previous study showing a weaker expression of P-gp in excised nasal mucosa compared to Caco-2 cells using the western blot technique [56]. Interestingly, two further studies have described a weak to moderate gene expression of P-gp in human nasal mucosa [18] and primary nasal cells [57]. The functional activity of this transporter was evaluated using rhodamine 123, a P-gp substrate

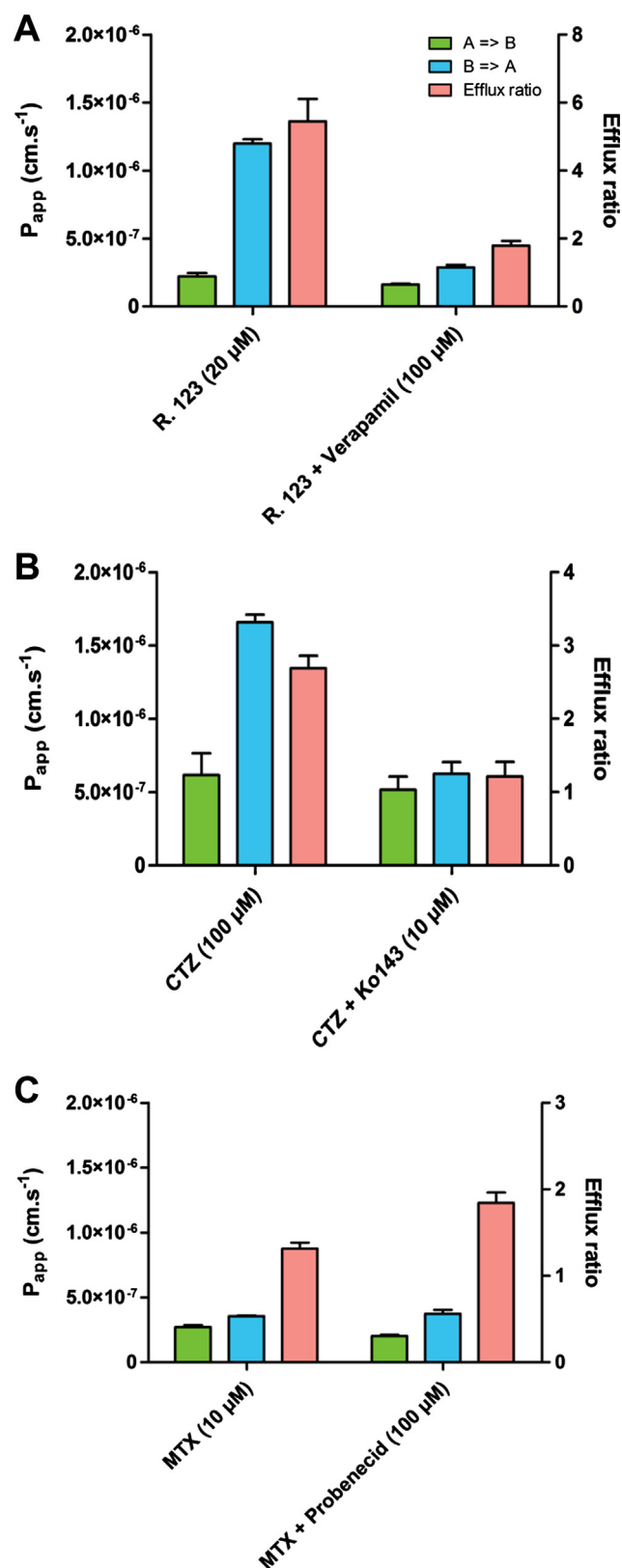


Fig. 4. Bidirectional permeability and efflux ratio of rhodamine 123 (A), chlorothiazide (B) and methotrexate (C) through the MucilAir™ nasal model after 2 h of incubation. P_{app} bidirectional permeability, R. 123: rhodamine 123, CTZ: chlorothiazide, MTX: methotrexate; $n = 3$ for each condition. Data are expressed as the mean \pm standard deviation.

previously shown to display an active efflux in intestinal Caco-2 cells [58]. We observed a dissymmetric transport of rhodamine 123 through MucilAir™, resulting in an ER of approximately 6 that was reduced by a factor of 3 in the presence of verapamil, a P-gp inhibitor [59]. As already reported, a compound may be considered as a substrate of ABC transporters if its ER is equal to or is above 2 and is at least halved in the presence of the corresponding selective inhibitor [4,60]. Based on this observation, P-gp was functional in the MucilAir™ nasal model and acted as an apical pump that reduced drug absorption by extruding xenobiotics out of the cells [61].

As a member of the ABC transporter family, BCRP also performs a detoxifying function, manifesting broad substrate specificity [62]. We showed that the apical expression of BCRP in the MucilAir™ nasal model follows the same pattern as in bronchial Calu-3 cells [63]. The expression of BCRP in the nasal mucosa has been little investigated. Only a moderate gene expression was demonstrated in a recent study [18] and this finding could be consistent with the weaker detection of BCRP in MucilAir™ compared to the Caco-2 model. Chlorothiazide was used as a substrate of BCRP in functional studies. This diuretic displayed an ER above 3 in the Caco-2 model [64] that was abolished by the known BCRP inhibitor Ko143 [65]. The bidirectional transport of chlorothiazide through MucilAir™ resulted in an ER of approximately 3. Addition of the inhibitor Ko143 halved the ER, thereby confirming the functional activity of BCRP in the nasal MucilAir™ model.

MRPs are ABC efflux pumps involved in the excretion of metabolized xenobiotic compounds from cells [66]. We successfully demonstrated the homogenous apical expression of MRP1 in the MucilAir™ model as previously described in human nasal epithelium [17]. The greater abundance of MRP1 in MucilAir™ compared to Caco-2 was in accordance with the results of a previous study reporting a much higher signal of MRP1 in excised nasal mucosa than in the Caco-2 cell line, using western blotting [67]. Moreover, MRP1 was found to be the most abundant isoform in human nasal mucosa [18] and primary nasal cells [57]. MRP2 showed a faint and heterogeneous lateral signal at all plasma membranes in accordance with its weak gene expression in both nasal epithelium and primary nasal cells [18,57]. A far weaker expression of MRP2 in the nasal mucosa than in the Caco-2 cell line was demonstrated using the western blot technique [67] strengthening the correlation between the MucilAir™ model and the nasal mucosa. Although both MRP1 and MRP2 were expressed in the MucilAir™ model, no active efflux of methotrexate was shown in functional studies. This could be explained by the opposite subcellular distribution of MRP1 and MRP2 at the apical and basolateral membrane, respectively. Considering that methotrexate is a broad-spectrum substrate of MRPs [68], the active efflux of this compound, mediated by MRP1 in the apical compartment, could be balanced by its excretion by MRP2 in the basal compartment, leading to the absence of a net active efflux. An alternative hypothesis refers to the simultaneous expression of MRP3, MRP4 and MRP7 in MucilAir™, these ABC transporters also being potentially involved in the active transport of methotrexate [69].

To the best of our knowledge, this study is the first to demonstrate the potent correlation between the MucilAir™ nasal model and the normal nasal epithelium, with regard to the histological characteristics, barrier properties and functional expression of ABC transporters. This model could be used to further evaluate the involvement of ABC transporters in the bioavailability of nasally administered drugs. However, care should be taken regarding its predictability of nasal drug absorption. The immortalized Caco-2 cell line is currently the gold-standard for the prediction of intestinal drug absorption due to strong *in vitro-in vivo* correlations [3]. We recently showed that the RPMI 2650 model may be a potential candidate but failed to anticipate the active efflux of drugs mediated by ABC transporters [20]. Although we demonstrated that the primary MucilAir™ model was morphologically and physiologically closer to the human nasal mucosa than the RPMI 2650 model, *in vitro-in vivo* correlations are still lacking to determine their predictability. Firstly, comparative studies with excised nasal mucosa

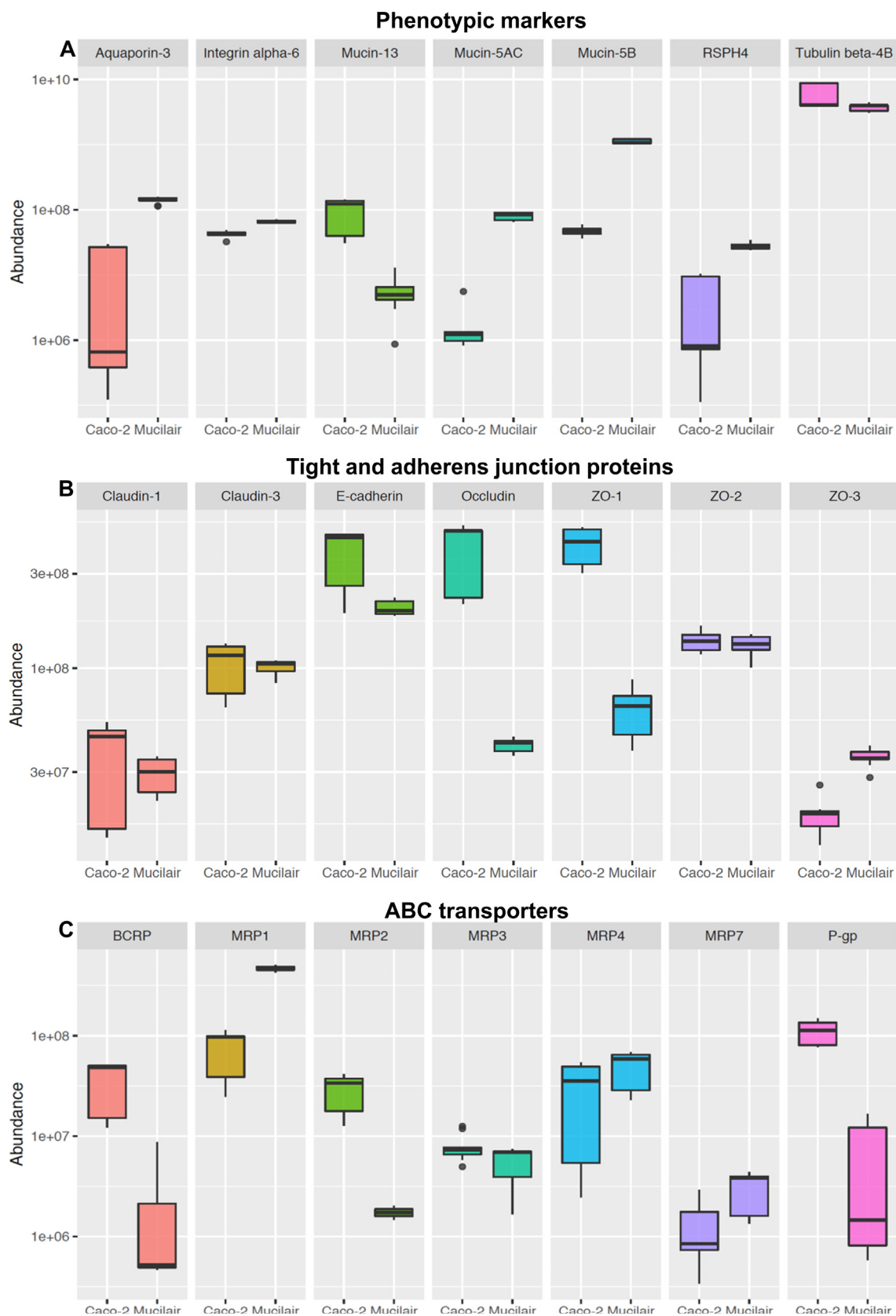


Fig. 5. Label-free quantification of phenotypic markers (A), tight and adherens junction proteins (B) and ABC transporters (C) in the MucilAir™ nasal and Caco-2 models. Whiskers indicate the first and third quartiles of the data, the horizontal bar within each box indicating the median value. Three biological replicates were examined for each model, each biological replicate being analyzed three times.

focused on drug transporters expression and both passive permeability and active efflux of reference compounds should be performed to confirm the relevance of the *in vitro* permeability data. Ultimately, the relationship between the *in vitro* permeability data and *in vivo* nasal absorption rates of reference drugs in humans must be evaluated to determine the relevance of MucilAir™ to accurately predict nasal drug absorption in pre-clinical studies.

5. Conclusion

This study reports the first original pharmacological characterization of the MucilAir™ nasal model in terms of morphology, phenotype and expression of tight and adherens junction proteins, as well as the functionality of ABC drug transporters. The MucilAir™ nasal model matched the major features of a normal human nasal epithelium. The homogeneous expression of tight and adherens junction proteins over the entire apical surface of the epithelium demonstrated the ability of MucilAir™ to form a polarized and hermetically sealed barrier. The ABC transporters P-gp, MRP1, MRP2 and BCRP were all expressed at different levels and exhibited distinct IF patterns in accordance with their subcellular localizations. Bidirectional transport studies demonstrated the functional activities of P-gp and BCRP, these transporters being capable of actively effluxing their respective substrates. Finally, the MucilAir™ nasal model could be used as a relevant tool in preclinical screening studies for evaluating the involvement of ABC transporters in the bioavailability of nasally administered drug candidates.

Acknowledgments

The authors thank Odile Sabido for conducting the flow cytometry experiments.

Funding sources

This research did not receive any specific grant from funding agencies in the public, commercial, or not-for-profit sectors.

Conflict of interest

C.M declare that S.C is the CEO of Epithelix SARL. S.C provided technical support and was not involved in the design of the study, the analysis of results and the writing of the article.

References

- [1] L. Illum, Nasal drug delivery—possibilities, problems and solutions, *J. Control. Release* 87 (2003) 187–198.
- [2] D. Zhang, G. Luo, X. Ding, C. Lu, Preclinical experimental models of drug metabolism and disposition in drug discovery and development, *Acta Pharm. Sin. B* 2 (2012) 549–561.
- [3] FDA guidance for industry. Drug interaction studies – study design, data analysis, and implications for dosing and labeling. Available at: <https://www.fda.gov/OHRMS/DOCKETS/98fr/06d-0344-gdl0001.pdf>. (accessed April 4, 2018).
- [4] A.W. McClurkin, E.C. Pirtle, M.F. Coria, R.L. Smith, Comparison of low- and high-passage bovine turbinate cells for assay of bovine viral diarrhoea virus, *Arch Gesamte Virusforsch* 45 (1974) 285–289.
- [5] A.T. Hood, D. Currie, S.J. Garte, Establishment of a rat nasal epithelial tumor cell line, *Vitro Cell Dev. Biol.* 23 (1987) 274–278.
- [6] C. Mercier, N. Perek, X. Delavenne, Is RPMI 2650 a suitable *in vitro* nasal model for drug transport studies? *Eur. J. Drug Metab. Pharmacokinet.* 43 (2017) 13–24.
- [7] P.S. Moorhead, Human tumor cell line with a quasi-diploid karyotype (RPMI 2650), *Exp. Cell Res.* 39 (1965) 190–196.
- [8] S. Dimova, M.E. Brewster, M. Noppe, M. Jorissen, P. Augustijns, The use of human nasal *in vitro* cell systems during drug discovery and development, *Toxicol. In Vitro* 19 (2005) 107–122.
- [9] A.A. Reus, W.J. Maas, H.T. Jansen, S. Constant, Y.C. Staal, J.J. van Triel, C.F. Kuper, Feasibility of a 3D human airway epithelial model to study respiratory absorption, *Toxicol. In Vitro* 28 (2014) 258–264.
- [10] S. Huang, L. Wiszniewski, S. Constant, E. Roggen, Potential of *in vitro* reconstituted 3D human airway epithelia (MucilAir™) to assess respiratory sensitizers, *Toxicol. In Vitro* 27 (2013) 1151–1156.
- [11] P. Arora, S. Sharma, S. Garg, Permeability issues in nasal drug delivery, *Drug Discov. Today* 7 (2002) 967–975.
- [12] S. Nickel, C.G. Clerkin, M.A. Selo, C. Ehrhardt, Transport mechanisms at the pulmonary mucosa: implications for drug delivery, *Expert Opin. Drug Deliv.* 13 (2016) 667–690.
- [13] M.M. Gottesman, T. Fojo, S.E. Bates, Multidrug resistance in cancer: role of ATP-dependent transporters, *Nat. Rev. Cancer* 2 (2002) 48–58.
- [14] G. Szakács, A. Váradi, C. Ozvegy-Laczka, B. Sarkadi, The role of ABC transporters in drug absorption, distribution, metabolism, excretion and toxicity (ADME-Tox), *Drug Discov. Today* 13 (2008) 379–393.
- [15] H. Sun, H. Dai, N. Shaik, W.F. Elmquist, Drug efflux transporters in the CNS, *Adv. Drug Deliv. Rev.* 55 (2003) 83–105.
- [16] G. Englund, F. Rorsman, A. Rönnblom, U. Karlbom, L. Lazorova, J. Gråsjö, A. Kindmark, P. Artursson, Regional levels of drug transporters along the human intestinal tract: co-expression of ABC and SLC transporters and comparison with Caco-2 cells, *Eur. J. Pharm. Sci.* 29 (2006) 269–277.
- [17] M.A. Wioland, J. Fleury-Feith, P. Corlieu, F. Commo, G. Monceaux, J. Lacau-St-Guilly, J.F. Bernaudin, CFTR, MDR1, and MRP1 immunolocalization in normal human nasal respiratory mucosa, *J. Histochem. Cytochem.* 48 (2000) 1215–1222.
- [18] M. Al-Ghabeish, T. Scheetz, M. Assem, M.D. Donovan, Microarray determination of the expression of drug transporters in humans and animal species used for the investigation of nasal absorption, *Mol. Pharm.* 12 (2015) 2742–2754.
- [19] A. Kocharyan, R. Feldman, A. Singleton, X. Han, B.S. Bleier, P-glycoprotein inhibition promotes prednisone retention in human sinonasal polyp explants, *Int. Forum Allergy Rhinol.* 4 (2014) 734–738.
- [20] C. Mercier, S. Hodin, Z. He, N. Perek, X. Delavenne, Pharmacological characterization of the RPMI 2650 model as a relevant tool for assessing the permeability of intranasal drugs, *Mol. Pharm.* 15 (2018) 2246–2256.
- [21] J. Metz, K. Knoth, H. Groß, C.M. Lehr, C. Stähler, U. Bock, M. Hittinger, Combining MucilAir™ and Vitrocell® powder chamber for the *in vitro* evaluation of nasal ointments in the context of aerosolized pollen, *Pharmaceutics* 10 (2018) 56.
- [22] B. De Servi, F. Ranzini, N. Piqué, Protective barrier properties of Rhinosectan® spray (containing xyloglucan) on an organotypic 3D airway tissue model (MucilAir): results of an *in vitro* study, *Allergy Asthma Clin. Immunol.* 13 (2017) 37.
- [23] F. Forest, G. Thuret, P. Gain, J.M. Dumollard, M. Peoc'h, C. Perrache, Z. He, Optimization of immunostaining on flat-mounted human corneas, *Mol. Vis.* 21 (2015) 1345–1356.
- [24] Z. He, N. Campolmi, B.M. Ha Thi, J.M. Dumollard, M. Peoc'h, O. Garraud, S. Piselli, P. Gain, G. Thuret, Optimization of immunolocalization of cell cycle proteins in human corneal endothelial cells, *Mol. Vis.* 17 (2011) 494–511.
- [25] K.M. Giacomini, S.M. Huang, D.J. Tweedie, L.Z. Benet, K.L. Brouwer, X. Chu, A. Dahlin, R. Evers, V. Fischer, K.M. Hillgren, K.A. Hoffmaster, T. Ishikawa, D. Keppler, R.B. Kim, C.A. Lee, M. Niemi, J.W. Polli, Y. Sugiyama, P.W. Swaan, J.A. Ware, S.H. Wright, S.W. Yee, M.J. Zamek-Gliszczynski, L. Zhang, Membrane transporters in drug development, *Nat. Rev. Drug Discov.* 9 (2010) 215–236.
- [26] H.C. Jensen-Smith, R.F. Ludueña, R. Hallworth, Requirement for the betaI and betaIV tubulin isotypes in mammalian cilia, *Cell Motil. Cytoskeleton* 55 (2003) 213–220.
- [27] B.W. Jafek, Ultrastructure of human nasal mucosa, *Laryngoscope* 93 (1983) 1576–1599.
- [28] C. Janke, The tubulin code: molecular components, readout mechanisms, and functions, *J. Cell Biol.* 206 (2004) 461–472.
- [29] A. Frommer, R. Hjejij, N.T. Loges, C. Edelbusch, C. Jahnke, J. Raidt, C. Werner, J. Wallmeier, J. Große-Onnebrink, H. Olbrich, S. Cindrić, M. Jaspers, M. Boon, Y. Memari, R. Durbin, A. Kolb-Kokocinski, S. Sauer, J.K. Marthin, K.G. Nielsen, I. Amirav, N. Elias, E. Kerem, D. Shoseyov, K. Haefner, H. Omran, Immunofluorescence analysis and diagnosis of primary ciliary dyskinesia with radial spoke defects, *Am. J. Respir. Cell Mol. Biol.* 53 (2015) 563–573.
- [30] J.F. McManus, Histological and histochemical uses of periodic acid, *Stain Technol.* 23 (1948) 99–108.
- [31] M.S. Ali, J.P. Pearson, Upper airway mucin gene expression: a review, *Laryngoscope* 117 (2009) 932–938.
- [32] D.M. Maher, B.K. Gupta, S. Nagata, M. Jaggi, S.C. Chauhan, Mucin 13: structure, function, and potential roles in cancer pathogenesis, *Mol. Cancer Res.* 9 (2011) 531–537.
- [33] A. Yaghi, M.B. Dolovich, Airway epithelial cell cilia and obstructive lung disease, *Cells* 5 (2016) 40.
- [34] A.G. Beule, Physiology and pathophysiology of respiratory mucosa of the nose and the paranasal sinuses, *Laryngorhinootologie* 89 (2010) 15–34.
- [35] J.R. Harkema, S.A. Carey, J.G. Wagner, The nose revisited: a brief review of the comparative structure, function, and toxicologic pathology of the nasal epithelium, *Toxicol. Pathol.* 34 (2006) 252–269.
- [36] S.M. Kreda, M.C. Gynn, D.A. Fenstermacher, R.C. Boucher, S.E. Gabriel, Expression and localization of epithelial aquaporins in the adult human lung, *Am. J. Respir. Cell Mol. Biol.* 24 (2001) 224–234.
- [37] P.R. Mills, R.J. Davies, J.L. Devalia, Airway epithelial cells, cytokines, and pollutants, *Am. J. Respir. Crit. Care Med.* 160 (1999) 38–43.
- [38] T. Kojima, M. Go, K. Takano, M. Kurose, T. Ohkuni, J. Koizumi, R. Kamekura, N. Ogasawara, T. Masaki, J. Fuchimoto, K. Obata, S. Hirakawa, K. Nomura, T. Keira, R. Miyata, N. Fujii, H. Tsutsumi, T. Himi, N. Sawada, Regulation of tight junctions in upper airway epithelium, *Biomed. Res. Int.* (2013), <https://doi.org/10.1155/2013/947072>.
- [39] J.M. Anderson, C.M. Van Itallie, Tight junctions and the molecular basis for regulation of paracellular permeability, *Am. J. Physiol.* 269 (1995) 467–475.
- [40] A. Hartsock, W.J. Nelson, Adherens and tight junctions: structure, function and connections to the actin cytoskeleton, *Biochim. Biophys. Acta* 1778 (2008) 660–669.

- [41] M. Furuse, M. Hata, K. Furuse, Y. Yoshida, A. Haratake, Y. Sugitani, T. Noda, A. Kubo, S. Tsukita, Claudin-based tight junctions are crucial for the mammalian epidermal barrier: a lesson from claudin-1-deficient mice, *J. Cell Biol.* 156 (2002) 1099–1111.
- [42] T. Hirase, J.M. Staddon, M. Saitou, Y. Ando-Akatsuka, M. Itoh, M. Furuse, K. Fujimoto, S. Tsukita, L.L. Rubin, Occludin as a possible determinant of tight junction permeability in endothelial cells, *J. Cell Sci.* 110 (1997) 1603–1613.
- [43] B.R. Stevenson, J.D. Siliciano, M.S. Mooseker, D.A. Goodenough, Identification of ZO-1: a high molecular weight polypeptide associated with the tight junction (zonula occludens) in a variety of epithelia, *J. Cell Biol.* 103 (1986) 755–766.
- [44] C.M. Niessen, C.J. Gottardi, Molecular components of the adherens junction, *Biochim. Biophys. Acta* 1778 (2008) 562–571.
- [45] G.A. Rogers, K. Den Beste, C.A. Parkos, A. Nusrat, J.M. Delgado, S.K. Wise, Epithelial tight junction alterations in nasal polyposis, *Int. Forum Allergy Rhinol.* 1 (2011) 50–54.
- [46] H.X. Ong, C.L. Jackson, J.L. Cole, P.M. Lackie, D. Traini, P.M. Young, J. Lucas, J. Conway, Primary air-liquid interface culture of nasal epithelium for nasal drug delivery, *Mol. Pharm.* 13 (2016) 2242–2252.
- [47] D.B. Price, M.L. Ackland, W. Burks, M.I. Knight, C. Suphioglu, Peanut allergens alter intestinal barrier permeability and tight junction localisation in Caco-2 cell cultures, *Cell Physiol. Biochem.* 33 (2014) 1758–1777.
- [48] J.L. Carson, A.M. Collier, M.R. Knowles, R.C. Boucher, Ultrastructural characterization of epithelial cell membranes in normal human conducting airway epithelium: a freeze fracture study, *Am. J. Anat.* 173 (1985) 257–268.
- [49] J.L. Madara, J.S. Trier, Structure and permeability of goblet cell tight junctions in rat small intestine, *J. Membr. Biol.* 66 (1982) 145–157.
- [50] S. Milatz, S.M. Krug, R. Rosenthal, D. Günzel, D. Müller, J.D. Schulzke, S. Amasheh, M. Fromm, Claudin-3 acts as a sealing component of the tight junction for ions of either charge and uncharged solutes, *Biochim. Biophys. Acta* 1798 (2010) 2048–2057.
- [51] A. Wengst, S. Reichl, RPMI 2650 epithelial model and three-dimensional reconstructed human nasal mucosa as in vitro models for nasal permeation studies, *Eur. J. Pharm. Biopharm.* 74 (2010) 290–297.
- [52] W. Hoffman, J. Gradinaru, L. Farcal, M. Caul-Futy, S. Huang, L. Wiszniewski, N. Parissus, S. Morath, S. Fortaner, T. Cole, E. Reginato, P.A. Carrupt, S. Constant, S. Coecke, Establishment of a human 3D tissue-based assay for upper respiratory tract absorption, *Appl. In Vitro Toxicol.* (2018), <https://doi.org/10.1089/aivt.2017.0035>.
- [53] D.A. Volpe, Drug-permeability and transporter assays in Caco-2 and MDCK cell lines, *Future Med. Chem.* 3 (2011) 2063–2077.
- [54] I. Hubatsch, E.G. Ragnarsson, P. Artursson, Determination of drug permeability and prediction of drug absorption in Caco-2 monolayers, *Nat. Protoc.* 2 (2007) 2111–2119.
- [55] U. Anand, A. Parikh, M.C. Ugwu, R.U. Agu, Drug transporters in the nasal epithelium: an overview of strategies in targeted drug delivery, *Future Med. Chem.* 6 (2014) 1381–1397.
- [56] A.M. Dolberg, S. Reichl, Expression of P-glycoprotein in excised human nasal mucosa and optimized models of RPMI 2650 cells, *Int. J. Pharm.* 508 (2016) 22–33.
- [57] M. Pozzoli, H.X. Ong, L. Morgan, M. Sukkar, D. Traini, P.M. Young, F. Sonvico, Application of RPMI 2650 nasal cell model to a 3D printed apparatus for the testing of drug deposition and permeation of nasal products, *Eur. J. Pharm. Biopharm.* 107 (2016) 223–233.
- [58] J. Zastre, J. Jackson, M. Bajwa, R. Liggins, F. Iqbal, H. Burt, Enhanced cellular accumulation of a P-glycoprotein substrate, rhodamine-123, by Caco-2 cells using low molecular weight methoxypolyethylene glycol-block-polycaprolactone diblock copolymers, *Eur. J. Pharm. Biopharm.* 54 (2002) 299–309.
- [59] M.A. Summers, J.L. Moore, J.W. McAuley, Use of verapamil as a potential P-glycoprotein inhibitor in a patient with refractory epilepsy, *Ann. Pharmacother.* 38 (2004) 1631–1634.
- [60] E.H. Kerns, L. Di, S. Petusky, M. Farris, R. Ley, P. Jupp, Combined application of parallel artificial membrane permeability assay and Caco-2 permeability assays in drug discovery, *J. Pharm. Sci.* 93 (2004) 1440–1453.
- [61] J.H. Lin, M. Yamazaki, Clinical relevance of P-glycoprotein in drug therapy, *Drug Metab. Rev.* 35 (2003) 417–454.
- [62] Q. Mao, J.D. Unadkat, Role of the breast cancer resistance protein (BCRP/ABCG2) in drug transport—an update, *AAPS J.* 17 (2015) 65–82.
- [63] D.K. Paturi, D. Kwatra, H.K. Ananthula, D. Pal, A.K. Mitra, Identification and functional characterization of breast cancer resistance protein in human bronchial epithelial cells (Calu-3), *Int. J. Pharm.* 384 (2010) 32–38.
- [64] E. Beéry, Z. Rajnai, T. Abonyi, I. Makai, S. Bánsághi, F. Erdő, I. Sziráki, K. Herédi-Szabó, E. Kis, M. Jani, J. Márki-Zay, G.K. Tóth, P. Krajcsi, ABCG2 modulates chlorothiazide permeability—in vitro-characterization of its interactions, *Drug Metab. Pharmacokinet.* 27 (2012) 349–353.
- [65] J.D. Allen, A. van Loevezijn, J.M. Lakhai, M. van der Valk, O. van Tellingen, G. Reid, J.H. Schellens, G.J. Koomen, A.H. Schinkel, Potent and specific inhibition of the breast cancer resistance protein multidrug transporter in vitro and in mouse intestine by a novel analogue of fumitremorgin C, *Mol. Cancer Ther.* 1 (2002) 417–425.
- [66] P. Borst, R. Evers, M. Kool, J. Wijnholds, A family of drug transporters: the multidrug resistance-associated proteins, *J. Natl. Cancer Inst.* 92 (2000) 1295–2302.
- [67] A.M. Dolberg, S. Reichl, Activity of multidrug resistance-associated proteins 1–5 (MRP1–5) in the RPMI 2650 cell line and explants of human nasal turbinate, *Mol. Pharm.* 14 (2017) 1577–1590.
- [68] G.D. Kruh, H. Zeng, P.A. Rea, G. Liu, Z.S. Chen, K. Lee, M.G. Belinsky, MRP subfamily transporters and resistance to anticancer agents, *J. Bioenergy Biomembr.* 33 (2001) 493–501.
- [69] Y.G. Assaraf, The role of multidrug resistance efflux transporters in antifolate resistance and folate homeostasis, *Drug Resist. Update* 9 (2006) 227–246.